

# Dual Drug Backboned Shattering Polymeric Theranostic Nanomedicine for Synergistic Eradication of Patient-Derived Lung Cancer

Yuwei Cong, Haihua Xiao, Hejian Xiong, Zigui Wang, Jianxun Ding, Chan Li, Xuesi Chen,\* Xing-Jie Liang,\* Dongfang Zhou,\* and Yubin Huang

**Most of the current nanoparticle-based therapeutics worldwide failing in clinical trials face three major challenges: (i) lack of an optimum drug delivery platform with precise composition, (ii) lack of a method of directly monitoring the fate of a specific drug rather than using any other labelling molecules as a compromise, and (iii) lack of reliable cancer models with high fidelity for drug screen and evaluation. Here, starting from a PP2A inhibitor demethylcantharidin (DMC) and cisplatin, the design of a dual sensitive dual drug backboned shattering polymer (DDBSP) with exact composition at a fixed DMC/Pt ratio for precise nanomedicine is shown. DDBSP self-assembled nanoparticle (DD-NP) can be triggered intracellularly to break down in a chain-shattering manner to release the dual drugs payload. Moreover, DD-NP with extremely high Pt heavy metal content in the polymer chain can directly track the drug itself via Pt-based drug-mediated computer tomography and ICP-MS both in vitro and in vivo. Finally, DD-NP is used to eradicate the tumor burden on a high-fidelity patient-derived lung cancer model for the first time.**

Development of nanoparticle (NP) drug delivery systems worldwide nowadays faces great problems and little progress was made in the last decades.<sup>[1]</sup> The major reason for the key bottleneck to the clinical translation of nanomedicine is due to three challenges. The first challenge is lack of optimum drug delivery platform with precise control over the drug composition,

carrier architectures as well as batch-to-batch variations in drug loading and/or release.<sup>[2]</sup> To achieve the precise control over carrier structure and drug composition in delivery systems either with a single drug, drug/drug or drug/gene combinations, people have developed drug initiated polymers,<sup>[3]</sup> chain shattering polymers containing drugs in the main chain as well as multifunctional hybrid drugs with multiple drugs in one molecule for drug delivery.<sup>[4]</sup> The second challenge is lack of way to direct monitor the fate of the specific drug itself rather than using any other molecules representing the drug for a compromise both in vitro and in vivo. To gain insight into the fate of such a nanoparticulate drug, people have developed numerous way of tracking by labeling either the drug and/or the carriers with fluorescent molecules via fluorescence imaging, iodine or heavy metal based contrast agents/NPs for magnetic resonance imaging (MRI)/positron emission tomography (PET)/CT imaging, upconversion imaging, etc., and a combination of them.<sup>[5]</sup> However, none of these methods is able to monitor the drug itself which is vital and of great interest for researchers. The third challenge is lack of reliable cancer models with high fidelity for drug screen and evaluation.<sup>[6]</sup>

Dr. Y. Cong, Dr. H. Xiao, Dr. H. Xiong, Dr. Z. Wang, Prof. D. Zhou, Prof. Y. Huang

State Key Laboratory of Polymer Physics and Chemistry  
Changchun Institute of Applied Chemistry  
Chinese Academy of Sciences  
Changchun 130022, P. R. China  
E-mail: east@ciac.ac.cn

Dr. Y. Cong, Dr. H. Xiao  
University of Chinese Academy of Sciences  
Beijing 100049, P. R. China

Dr. Z. Wang  
University of Science and Technology of China  
Hefei 230026, P. R. China

Dr. J. Ding, Prof. X. Chen

Key Laboratory of Polymer Ecomaterials  
Changchun Institute of Applied Chemistry  
Chinese Academy of Sciences  
Changchun 130022, P. R. China  
E-mail: xschen@ciac.ac.cn

Dr. C. Li, Prof. X.-J. Liang  
Chinese Academy of Sciences (CAS) Center for Excellence in  
Nanoscience and Laboratory of Controllable Nanopharmaceuticals  
CAS Key Laboratory for Biomedical Effects  
of Nanomaterials and Nanosafety  
National Center for Nanoscience and Technology  
Beijing 100190, P. R. China  
E-mail: liangxj@nanoctr.cn

 The ORCID identification number(s) for the author(s) of this article can be found under <https://doi.org/10.1002/adma.201706220>.

DOI: 10.1002/adma.201706220

Currently widely used in vitro cell culture systems are advantageous for routine experimental use. However, the cells are often passaged for hundreds of times which are lack of high fidelity without representation of cancer heterogeneity and complexity of tumor microenvironment.<sup>[7]</sup> Nevertheless, patient-derived cancer xenograft (PDX) models are such models bearing great similarity to tumors in clinic such as tumor architecture, cancer cells cross-talk and interactions, and acidic tumor microenvironment.<sup>[8]</sup> Therefore, PDX models are considered as high-fidelity models which can represent the heterogeneous nature of cancers.<sup>[9]</sup> Worldwide translation research of novel drugs as well as NP-based cancer therapeutics is often plagued due to the discrepancies between preclinical and clinical trials. This could be attributed to the cancer models which are lack of clinical relevance and high-fidelity models such as PDX models are therefore in great need.

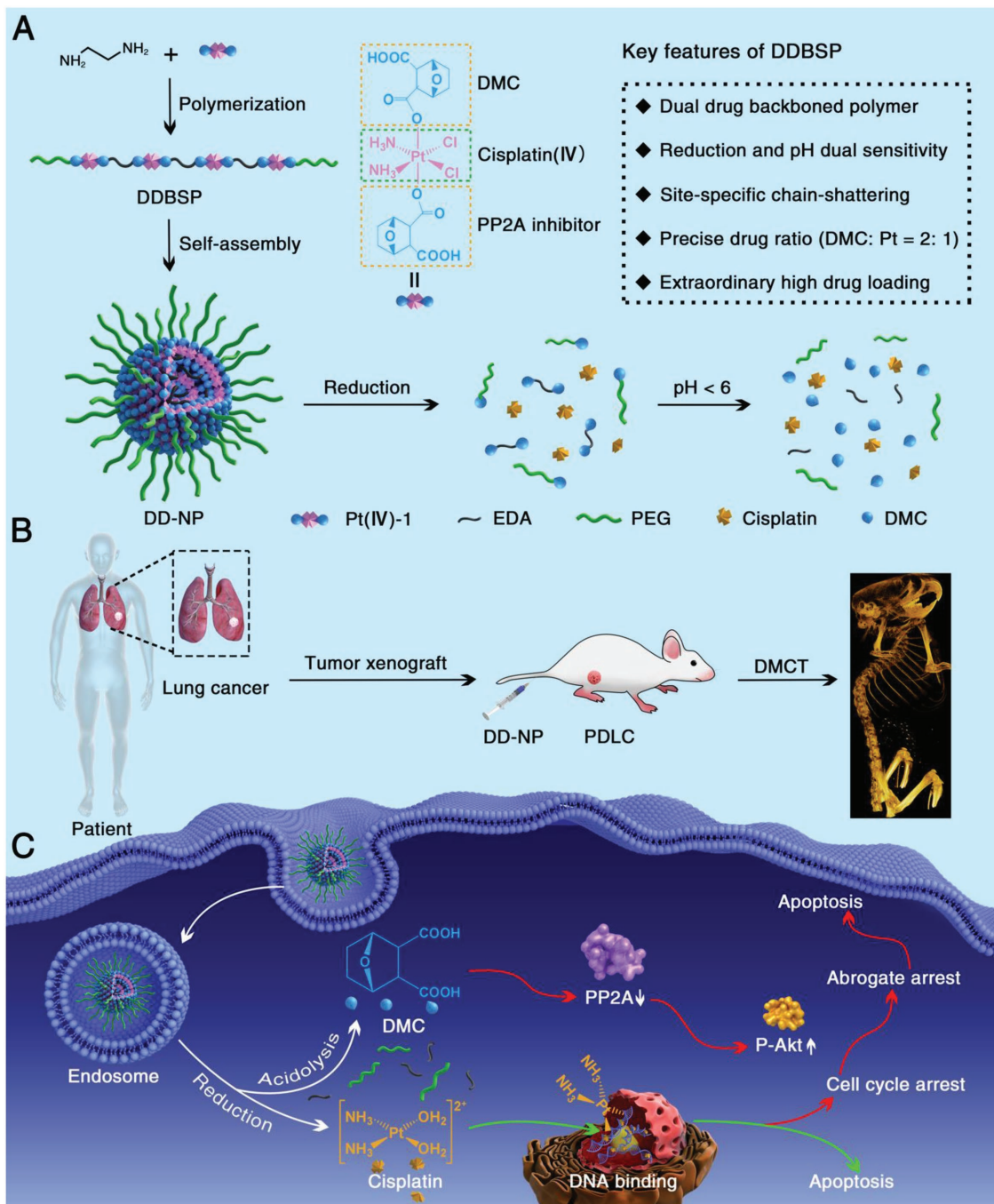
Effective chemotherapy is achieved when drugs are given in combination.<sup>[10]</sup> Drugs with different mechanisms are used in combination chemotherapy to work in a concerted way or overcome cancer resistance.<sup>[11]</sup> Cisplatin is widely used for treating more than 50% of cancers in clinic.<sup>[12]</sup> Recently, demethylcantharidin (DMC), as protein phosphatase 2A (PP2A) inhibitor, showed enhanced antitumor activity with DNA-damaging agents by specifically inhibition of PP2A without evident acute or chronic toxicity.<sup>[13]</sup> Previous studies have shown that combination use of cisplatin and DMC could synergize cancer therapy.<sup>[14]</sup>

To start with, cisplatin and DMC were found to be optimized at the ratio of 1:2 in combination use (Figure S1, Supporting Information), making it rational and imperative to keep this specific ratio till drugs enter the cells. Here, to tackle the above-mentioned three challenges, we therefore designed a dual sensitive dual drug backboned shattering polymer (DDBSP) with the dual drugs in its backbone. DMC was introduced to Pt(IV) drug which were then polymerized with ethylenediamine (EDA) into DDBSP that self-assembled into NPs (DD-NP; Scheme 1). The key features in DDBSP and DD-NP include: (i) Dual synergistic drugs were combined at a fixed and precise ratio in DD-NP for precise nanomedicine with extraordinary high drug loading that can hardly be achieved in other delivery systems via conventional drug conjugation/encapsulation. (ii) The backbone-type polymer was site-specifically chain-shattered via reduction of Pt(IV) to Pt(II) and acidolysis of DMC-containing  $\beta$ -carboxylic amide to DMC in the endosomal/lysosomal reductive and acidic microenvironments, making the drug release in a controlled but triggered manner.<sup>[14,15]</sup> (iii) The exceptional high content of Pt heavy metals in the polymer chain assures possible monitoring of the spatial/temporal dynamic distribution as well as metabolism of NPs via Pt-based drug-mediated computer tomography (DMCT). The iodine-free theranostic platform via DMCT differed from any NP systems reported till far as the anticancer Pt drug itself worked as CT imaging agent because there is no need for additional conventionally used fluorescent molecules and other MRI/CT/PET imaging agents. (iv) DD-NP was found to be able to eradicate the tumor burden on a patient-derived lung cancer (PDLC) model. PDLC faithfully reproduced the patient's original tumors for tumor heterogeneity, microenvironment, and genetic alterations hence replicated the real response to therapeutics. Hence, our results

provided the first example of precise nanomedicine tackling these three challenges for high fidelity PDLC, which could provide insights into the selection of patients, identifying those who can benefit from those treatments.

To construct DDBSP, a dual drug prodrug with both DMC and cisplatin was synthesized (Pt(IV)-1; Scheme S1, Supporting Information). As a comparison, a similar single drug prodrug compound with succinic acid and cisplatin was also prepared (Pt(IV)-2; Scheme S2, Supporting Information). Pt(IV)-1 has a fixed ratio of DMC/Pt at 2 combined in one molecule. Pt(IV)-2, however, only has Pt in its molecule. Thereafter, Pt(IV)-1 and Pt(IV)-2 were systematically characterized by <sup>1</sup>H-NMR, <sup>13</sup>C-NMR, high performance liquid chromatography (HPLC), electrospray interface mass spectrometer (ESI-MS), FTIR, and elemental analysis (Figures S2–S6 and Table S1, Supporting Information) and the successful synthesis of them was proved. These two prodrugs could be then polymerized with EDA via 1-ethyl-3-(3-dimethylaminopropyl)carbodiimide hydrochloride/N-hydroxysuccinimide (EDC.HCl/NHS) coupling to lose water molecules and form amide groups in a stepwised manner<sup>[4f]</sup> (Schemes S3 and S4, Supporting Information). Note, polymer that formed from Pt(IV)-1 can be called dual drug backboned shattering polymer, however, polymer that formed from Pt(IV)-2 can be called single drug backboned shattering polymer (SDBSP). Further characterization of DDBSP and SDBSP by <sup>1</sup>H-NMR, IR, and gel permeation chromatography (GPC) proves the formation of polymers (Figures S7–S9 and Table S2, Supporting Information). The molecular weight of both polymers is  $\approx$ 7500 with high Pt content at 12.3 wt% (DDBSP) and 16.3 wt% (SDBSP), corresponding to a cisplatin drug content at 20.9 wt% and 27.8 wt%, respectively. Both DDBSP and SDBSP can readily self-assemble into nanoparticles (DD-NP and SD-NP) in water with poly(ethylene glycol) (PEG) in the corona and the drugs in the core (Schemes S5 and S6, and Figures S7B, S8B, Supporting Information).

Pt(IV) prodrugs are known to be reduction-sensitive to release toxic Pt(II) by sodium ascorbate and/or glutathione overexpressed in tumor cells.<sup>[12]</sup> Here, this reduction-sensitive release came from the nature of Pt(IV) chemistry indicated by a relative low reduction potential of both DD-NP and SD-NP at pH 5.0 (0.542 and 0.681 V, respectively) and pH 7.4 (0.592 and 0.62 V, respectively) (Figure 1A,B; Figures S10–S12, Supporting Information). Rapid breakdown of the polymer chain and release of the drug payload in the cancer cells is vital for the anticancer activity. Representative dissociation process of DD-NP via reduction can be visualized by transmission electron microscopy (TEM) (Figure 1C). From 0 to 24 h in the presence of  $5 \times 10^{-3}$  M sodium ascorbate, DD-NP with an original size at 180 nm by transmission electron microscopy (TEM) fell apart to pieces which formed both smaller nanoparticles at 150 nm and aggregated as large particles at 500 nm at first. Later, large particles were eventually broken down to tiny ones (50 nm).<sup>[4e]</sup> This process could be further supported by the shift of DLS signal of original NPs at a single peak at 182 nm to dual peaks at 126 and 291 nm at 2 h, and eventually to a single peak at 60 nm at 24 h (Figure 1D). No obvious changes of the morphology and size of DD-NP were observed at pH 7.4 and 5.0 for 24 h (Figure S13, Supporting Information), indicating the stability for long circulation.<sup>[4c,16]</sup> In the presence of sodium



**Scheme 1.** Schematic illustration of dual drug backboned shattering polymeric theranostic nanomedicine (DDBSP) for synergistic eradication of patient-derived lung cancer (PDLC). A) Illustration of structure of Pt(IV)-1, polymerization of DDBSP, self-assembly and chain-shattering of DD-NP to release active Pt(II) and DMC, and key features of DDBSP and DD-NP. B) Illustration of establishment of PDLC model and Pt-based DMCT after intravenously injection with DD-NP. C) Possible dual anticancer mechanisms after endocytosis of DD-NP by cancer cells.

ascorbate, the GPC curves of DDBSP widened with time and showed a group of low molecular-weight species, demonstrating the reduction-sensitive degradation of the synthesized polymer (Figure 1E). As the Pt(IV) reduction process took only 30 min to 12 h, the Pt(IV) species in the main chain of both DDBSP and SDBSP, were the driving force to make rapid breakdown of the polymers via a chain-shattering manner. To

quantify this process, 81.9% release of Pt drug within 3 h triggered by  $5 \times 10^{-3}$  M sodium ascorbate was observed by ICP-MS (Figure 1F). Pt(II) rather Pt(IV) act as final DNA crosslinking agents, resulting in inhibition of DNA replication and eventual cell apoptosis and death.<sup>[12]</sup> We therefore showed that the Pt(IV) in DDBSP (binding energies for Pt<sub>4f</sub>, 78.4 and 75.2 eV) was completely reduced to Pt(II) (binding energies for Pt<sub>4f</sub>,

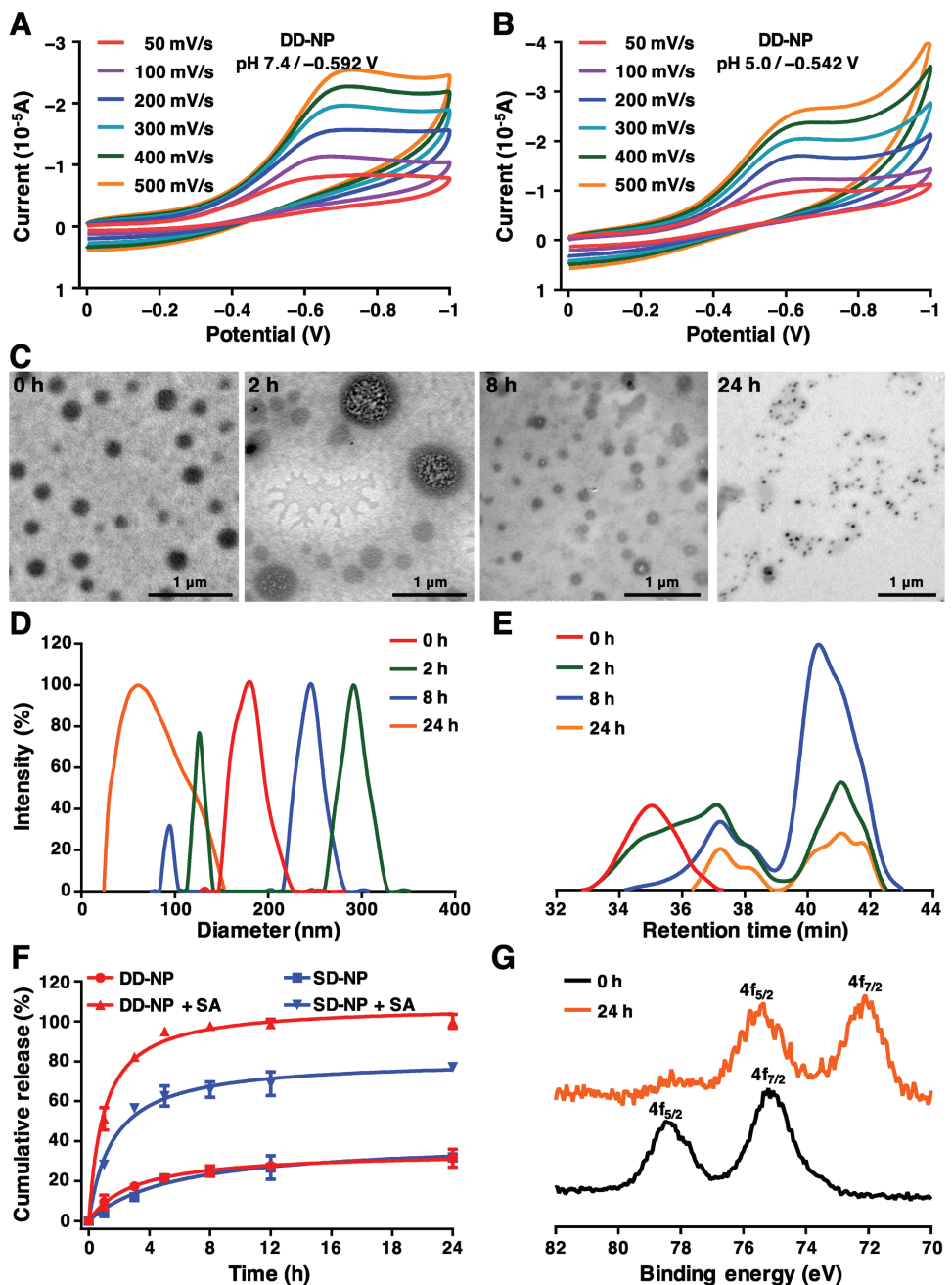


**Figure 1.** Characterization of reduction-sensitive DDBSP self-assembled DD-NP. Cyclic voltammograms of DD-NP in 0.1 M KCl solution at A) pH 7.4 and B) pH 5.0 with varied scan rates. C) TEM images, D) hydrodynamic diameters and E) GPC traces of DD-NP in response to sodium ascorbate (SA,  $5 \times 10^{-3}$  M) for 0, 2, 8, and 24 h. F) Pt release profiles of DD-NP and SD-NP in water with or without SA ( $5 \times 10^{-3}$  M). G) XPS curves of Pt<sub>4f</sub> before and after incubation with SA ( $5 \times 10^{-3}$  M) for 24 h.

75.5 and 72.0 eV) by X-ray photoelectron spectroscopy (XPS) (Figure 1G).<sup>[4e]</sup> The whole process was similar for SDBSP (Figures S14,S15, Supporting Information), further suggesting the reduction-sensitivity of Pt(IV) backboned polymers. Finally, we proved the released Pt can form bis-adducts ( $\text{NH}_3^+$ ) $\text{Pt}(\text{5}'\text{-GMP})_2$  at m/z equal to 903.5 and  $\text{Pt}(\text{5}'\text{-GMP})_2$  at m/z equal to 884.1 with a key Pt target molecule in DNA strand, 5'-GMP by ESI-MS for both DDBSP and SDBSP (Figures S16,S17, Supporting Information).

The cellular internalization of polymeric NPs is usually mediated by endocytosis (Figure S18, Supporting Information), which can promote the drug uptake.<sup>[16]</sup> As both DDBSP and SDBSP have Pt atoms in the polymer main chain, making it possible to quantify the intracellular uptake of drugs by ICP-MS. As shown in Figure 2A, both free Pt(IV)-1 and DD-NP showed time-dependent increase in drug uptake on HeLa and A549 cell lines. However, DD-NP ( $135.69 \pm 2.80$  and  $138.32 \pm 8.22$  ng Pt mg<sup>-1</sup> protein) obviously had up to 3.7-fold and

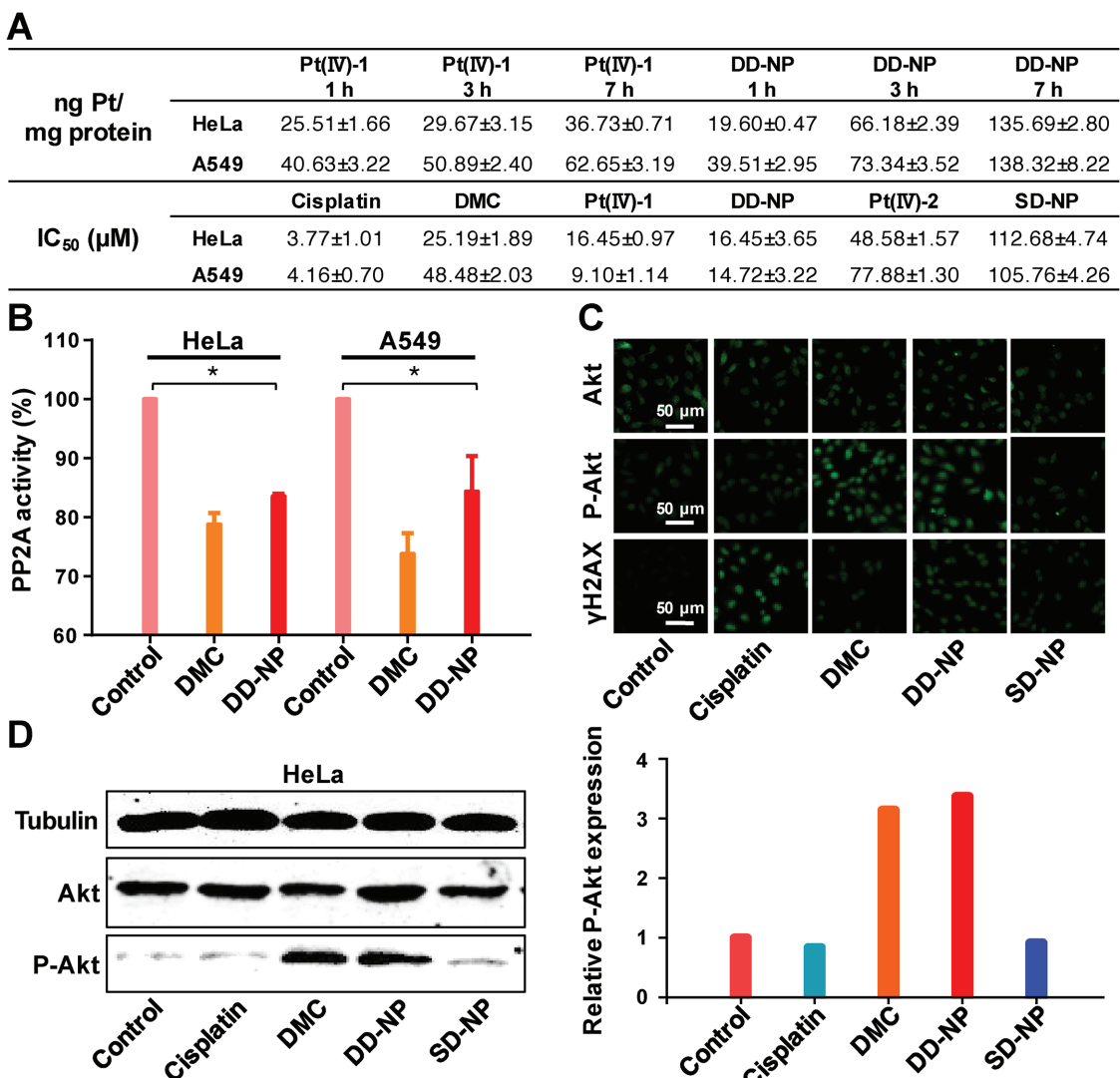


**Figure 2.** In vitro cytotoxicity profiles and action mechanism of DD-NP. A) Intracellular platinum uptake of HeLa and A549 cells after incubation of Pt(IV)-1 and DD-NP for 1, 3, and 7 h (detected by ICP-MS), and IC<sub>50</sub> values of cisplatin, DMC, Pt(IV)-1, DD-NP, Pt(IV)-2, and SD-NP against HeLa and A549 cells for 72 h. B) PP2A activity of HeLa and A549 cells after 6 h incubation of DMC ( $65 \times 10^{-6}$  M) and DD-NP ( $65 \times 10^{-6}$  M DMC). C) Immunofluorescence of Akt, P-Akt, and  $\gamma$ H2AX in A549 cells after exposure to cisplatin ( $2.5 \times 10^{-6}$  M), DMC ( $5 \times 10^{-6}$  M), DD-NP ( $2.5 \times 10^{-6}$  M Pt) and SD-NP ( $2.5 \times 10^{-6}$  M Pt) for 24 h. D) Western blot and relative P-Akt expression of HeLa cells after exposure to cisplatin ( $2.5 \times 10^{-6}$  M), DMC ( $5 \times 10^{-6}$  M), DD-NP ( $2.5 \times 10^{-6}$  M Pt/5  $\times 10^{-6}$  M DMC) and SD-NP ( $2.5 \times 10^{-6}$  M Pt) for 24 h. Significance is defined as \* $p < 0.05$ .

2.2-fold more uptake than Pt(IV)-1 ( $36.73 \pm 0.71$  and  $62.65 \pm 3.19$  ng Pt mg<sup>-1</sup> protein) for HeLa and A549 cell lines at 7 h, respectively, suggesting that NPs were beneficial for cancer cell accumulation and uptake. We further screened DD-NP in comparison to various agents by MTT assay on HeLa and A549 cell lines (Figure S19, Supporting Information). The IC<sub>50</sub> values were collected and summarized in Figure 2A (Table S3, Supporting Information). Specifically, DD-NP showed comparable efficacy to Pt(IV)-1 but was definitely better than SD-NP. For instance, the IC<sub>50</sub> value of DD-NP ( $14.72 \times 10^{-6}$  M) against A549 cell line for 72 h was over seven times lower than that of SD-NP ( $105.76 \times 10^{-6}$  M). Due to Pt(IV) rather than Pt(II) was in combination with DMC, DD-NP ( $(14.72 \pm 3.22) \times 10^{-6}$  and  $(16.5 \pm 3.65) \times 10^{-6}$  M) was less effective than cisplatin ( $(3.77 \pm 1.01) \times 10^{-6}$  and  $(4.16 \pm 0.70) \times 10^{-6}$  M) against HeLa and A549

cell lines for 72 h in vitro, respectively. The synergy effect should be evaluated based on the in vivo benefit which may come from the better accumulation of DD-NP via enhanced permeability and retention effect and lower systemic toxicity.<sup>[1a]</sup>

DMC can activate Akt pathway by inhibition of PP2A.<sup>[14]</sup> Increased expression of hyper-phosphorylation of Akt (P-Akt) would induce apoptosis from continued cell cycle progression.<sup>[13]</sup> Cisplatin is a widely used cancer chemotherapeutic drug that causes DNA crosslinking and stimulates  $\gamma$ H2AX phosphorylation.<sup>[17]</sup> To further demonstrate the combinational benefits and mechanism of action in vitro, the PP2A activity after treatment of various drugs was quantified by a Ser/Thr phosphatase assay. Both DMC and DD-NP can reduce the PP2A activity of HeLa and A549 cell lines to 15% to 20%, indicating the hydrolyzed release of DMC in the intracellular

acidic condition (Figure 2B).<sup>[14]</sup> Thereafter, we performed western blotting and immunofluorescence assays on HeLa and A549 cell lines after drug treatment for 24 h (Figure 2C,D; Figures S20,S21, Supporting Information). All the cells showed the same expression of tubulin and total Akt. Compared to cisplatin and SD-NP, DMC and DD-NP induced higher expression of P-Akt through PP2A inhibition. Finally, the DNA damage marker  $\gamma$ H2AX can be visualized by immunostaining the cells (Figure 2C; Figure S20, Supporting Information). Results showed that DD-NP induced the highest expression of  $\gamma$ H2AX expression in both cell lines after treatment for 24 h, indicating the severe genomic DNA damage.

To demonstrate the *in vivo* fate of DD-NP, we evaluated firstly its biodistribution on an extremely aggressive cervical cancer model (U14). After 24 h of a single intravenous (i.v.) injection at 2.5 mg Pt kg<sup>-1</sup>, results indicated that DD-NP achieved > threefold higher Pt concentration in tumor tissue than that of cisplatin measured by ICP-MS ( $2.06 \pm 0.59 \mu\text{g g}^{-1}$  vs  $0.63 \pm 0.04 \mu\text{g g}^{-1}$ ; Figure S22, Supporting Information). To evaluate the safety of DD-NP, toxicity studies based on histopathological analysis by H&E staining of tissue sections isolated from KM mice at day 18 after three times injection indicated that no significant morphological changes were detected in heart, spleen, and lung in all the treated groups compared with the saline group. Further abundant inflammatory cell infiltration and edema with thickening of the glomerular basement membrane in cisplatin, DMC, and Pt(IV)-2 treated mice indicated severe nephrotoxicity. However, both DD-NP and SD-NP-treated mice displayed no noticeable signals of damage on liver and kidney (Figure S23, Supporting Information), indicating the safety of them. It is reasonable that the inert Pt(IV) prodrug form in these NPs and further polymerization of Pt(IV) prodrug into polymer backbones would concurrently conceal the systemic toxicity from cisplatin(II).<sup>[4a,c,18]</sup>

To find out whether the better accumulation of DD-NP and lower toxicity could result in maximized efficacy, we then first screened the drugs on KM mice bearing subcutaneous U14 model. Results showed that DD-NP had the best tumor inhibition ability (Figure 3A). SD-NP without DMC was less potent than DD-NP, indicating the synergy of DMC with Pt *in vivo*. Specifically, the tumor size was about 750 mm<sup>3</sup> in DD-NP group while 2100 mm<sup>3</sup> in SD-NP group after 18 d. Cisplatin is known to severely damage kidneys hence it is toxic to animals.<sup>[19]</sup> Here all the tested mice groups demonstrated 13.3% to 16.2% body weight increase except cisplatin treated one with 14.8% body weight loss at day 8, indicating the lower systemic toxicity of DD-NP than cisplatin (Figure 3B). What is more, the survival rate of DD-NP at day 18 kept 100%, which was obviously larger than other groups ranging from 57.1% to 85.7% (Figure 3C). At the end of day 18, the mice were then all sacrificed and bloods as well as tumors were collected from the remaining mice. The higher levels of blood biochemistry parameters CREA, UA, and UREA at day 18 resulting from cisplatin and Pt(IV)-1 treated mice than control and DD-NP groups indicated the severe renal toxicity induced by free small drugs (Figure 3D).<sup>[20]</sup> Photo of U14 tumors and mean tumor weight after tumor dissection from mice demonstrated that DD-NP inhibited tumor growth to 1/5 of the nontreated group (PBS) and 1/3 of Pt(IV)-1 treated group (Figure 3E,F). Finally,

to find out the mechanism of action of DD-NP *in vivo*, TUNEL and H&E staining of tumor sections isolated from mice at day 18 were performed. For TUNEL assay, nuclei were labeled with Hoechst 33258 (blue) and broken DNA strands were stained by FITC (green) (Figure 3G). DD-NP group showed extensive and much more regions of apoptosis cells than other groups. Furthermore, in H&E assay, the extensive nuclear shrinkage, fragmentation, and absence were observed in DD-NP group, which was possibly the reason that resulted in the most significant declination of the tumor.

X-ray CT is an important diagnostic imaging technique due to its high resolution and deep tissue penetration.<sup>[21]</sup> DDBSP with uniquely high Pt contents (20.9% based on cisplatin) in the polymer main chain, makes it possible for Pt-based DMCT which allows the spatial temporal monitoring the dynamic distribution of Pt drugs as well as the NPs. As shown in Figure 4A, after 1 h i.v. injection of DD-NP at 10 mg Pt kg<sup>-1</sup> into KM mice bearing U14 model, a lot of white dots emerged and still existed even after 24 h in the front and side views, while no white dots showed in the control mice, indicating the long circulation ability of DD-NP (Figure S24, Supporting Information). Ex vivo CT images of organs (background subtracted, Figure 4B) demonstrated clearly the accumulation of Pt drugs in tumor with time as revealed by the distributed white dots both in the periphery and core of the tumor. The white dots in the core of tumor indicated the penetration of DD-NP to the tumor core. To quantify this, Hounsfield units (HU) value by CT and ICP-MS of the ultimate Pt content in the tissues and organs was collected for comparison (Figure 4C,D). Overall, the relative pattern of distribution of DD-NP by two methods was similar except heart. Specifically, the gradual decreased HU signals for liver could be observed with time from 1 h (83.3 HU) to 6 h (63.8 HU), 12 h (51.7 HU), and 24 h (20.2 HU). With both methods, we can clearly see the great increase from 3.51  $\mu\text{g Pt g}^{-1}$  (3.24 HU) to 10.20  $\mu\text{g Pt g}^{-1}$  (57.14 HU) from 1 to 24 h in the tumor sites.

Moreover, instead of using U14 model, which differs a lot from patient cancers in clinic, and makes the preclinical evaluation of drugs less reliable, we here established PDLC model obtained by direct implantation of lung cancer tissue fragments in immunocompromised BALB/c mice. The PDLC model faithfully reproduced the patient's original tumor and the environment as well as the heterogeneity and genetic mutations proved by H&E assay (Figure S25, Supporting Information). Hence, the modulation of PDLC with DD-NP could give more insight into the use of Pt nanomedicine in lung cancer. Mice with PDLC model were further CT imaged after i.v. injection of DD-NP at 10 mg Pt kg<sup>-1</sup> for 1, 12, and 24 h. We can clearly see the white dots, which could be assigned to Pt loaded NPs distributed majorly in the abdomen and the excised organs (Figure S26A,B, Supporting Information). Moreover, the CT signals were correlated very well to the average HU signals (Figure S26C, Supporting Information) and absolute platinum biodistribution measured by ICP-MS (Figure S26D, Supporting Information). For tumour tissue, the CT signals and Pt concentrations were 12.81 HU and 0.84  $\mu\text{g Pt g}^{-1}$  at 1 h, 35.50 HU and 3.90  $\mu\text{g Pt g}^{-1}$  at 24 h, respectively, demonstrating the accumulation of NPs and Pt at the tumour site.

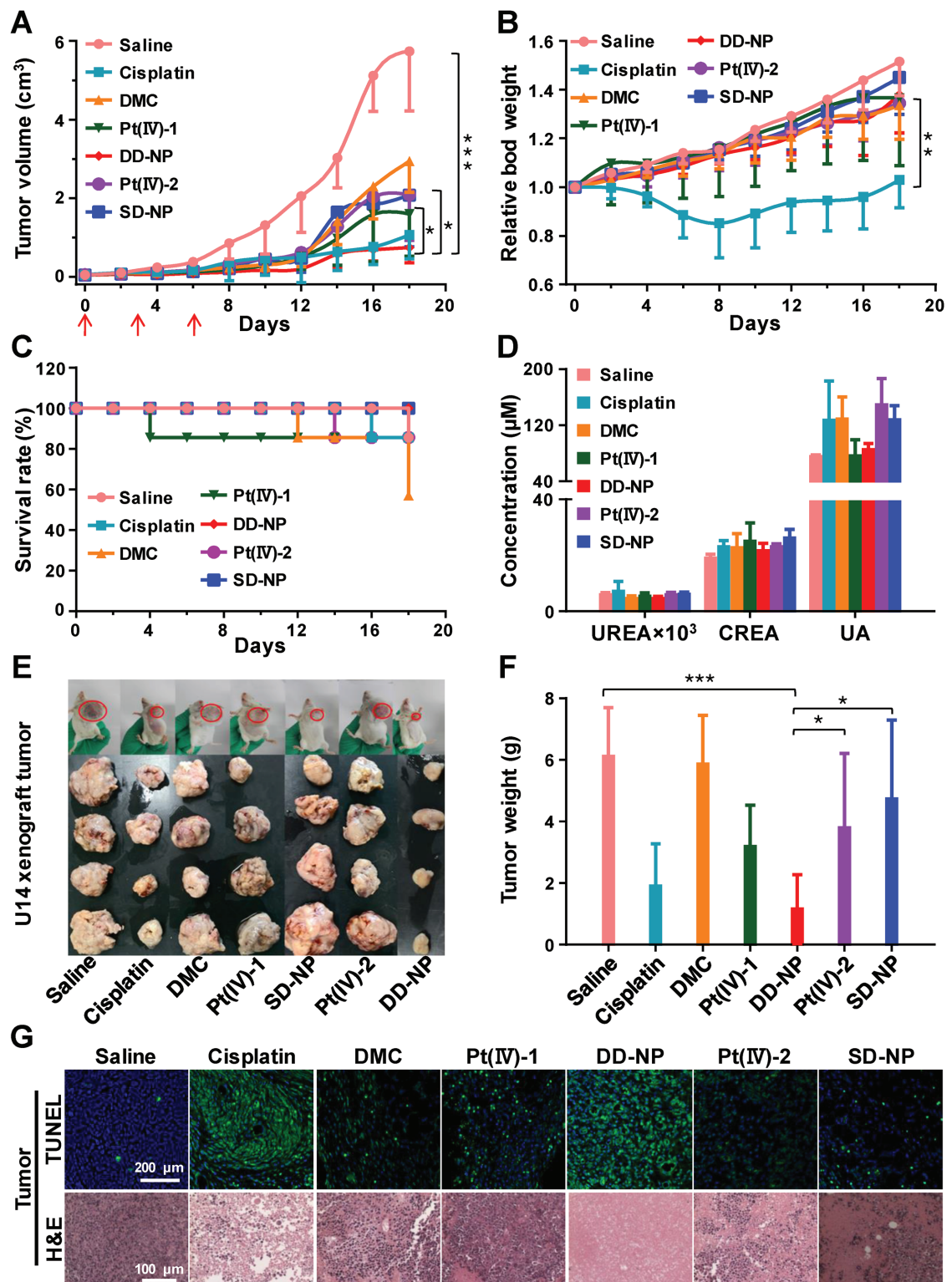


**Figure 3.** In vivo antitumor efficacy, toxicity, and action mechanism of DD-NP on KM mice bearing subcutaneous U14 tumor model. The KM mice were administered intravenously with saline, cisplatin (2 mg Pt kg<sup>-1</sup>), DMC (3.36 mg kg<sup>-1</sup>), Pt(IV)-1 (2 mg Pt kg<sup>-1</sup>), DD-NP (2 mg Pt kg<sup>-1</sup>), Pt(IV)-2 (2 mg Pt kg<sup>-1</sup>) and SD-NP (2 mg Pt kg<sup>-1</sup>) on days 0, 3, and 6. A) Tumor growth curve, B) body weight change and C) survival rate of mice during the test. D) Alterations of CREA, UA, and UREA of mice on day 18. E) Photo and F) tumor weight of U14 tumors isolated from mice on day 18. Data represent mean ± SD ( $n = 7$ ). G) TUNEL and H&E staining of tumor sections isolated from mice on day 18. For TUNEL assay, nuclei were stained by Hoechst 33258 (blue) and broken DNA strands were stained by FITC (green).

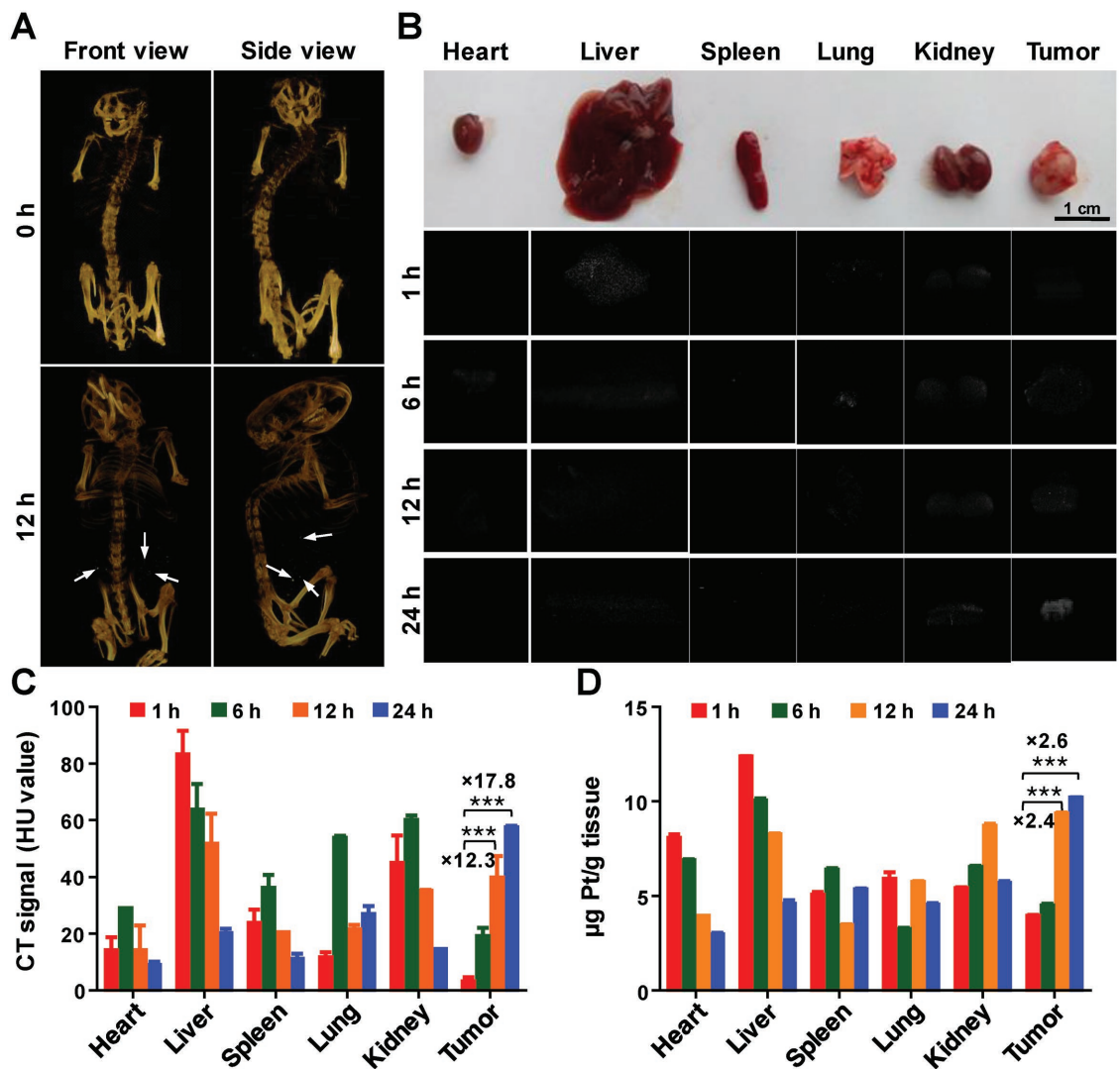


**Figure 4.** Directly tracking drug fate of DD-NP via Pt-based DMCT imaging on KM mice bearing subcutaneous U14 tumor model. A) In vivo CT images of mice before and after 12 h single intravenous administration of DD-NP ( $10 \text{ mg Pt kg}^{-1}$ ). The CT signals are indicated by the arrows. B) Ex vivo photo image and CT images of tissues isolated from mice after 1, 6, 12, and 24 h single intravenous administration of DD-NP ( $10 \text{ mg Pt kg}^{-1}$ ), and the control tissue background was deducted. Biodistribution of platinum in mice detected by (C) CT and (D) ICP-MS after single intravenous administration of DD-NP ( $10 \text{ mg Pt kg}^{-1}$ ) for 1, 6, 12, and 24 h. Significance is defined as \*\*\* $p < 0.001$ .

The anticancer efficacy of DD-NP on the above PDLC model was further evaluated. Among all the drugs, DD-NP were the most potent on inhibition of tumor growth (Figure 5A) but showed least effect on loss of mice body weight (Figure 5B) and higher survival rate (Figure S27, Supporting Information). Specifically, the average tumor volume of saline group increased to over  $3000 \text{ mm}^3$  after 7 weeks, while the tumor growth was well restricted without excessive growth volume in DD-NP group ( $330 \text{ mm}^3$ ). At day 51, all the mice were sacrificed and tumor nodules were collected and weighed. Mice treated with DD-NP had the smallest tumors (Figure 5C), which was 1/6 of the PBS treated group and 1/2 of cisplatin and SD-NP groups (Figure 5D). To unveil the efficacy study, lysis of the tumor for Pt accumulation in the tumor and Pt-DNA adducts formed by ICP-MS indicated DD-NP had the most Pt accumulation ( $2.09 \mu\text{g Pt g}^{-1}$  tumor) as compared to  $1.37 \mu\text{g Pt g}^{-1}$  tumor for

cisplatin) and Pt-DNA adducts ( $0.84 \mu\text{g Pt g}^{-1}$  tumor DNA as compared to  $0.53 \mu\text{g Pt g}^{-1}$  tumor DNA for cisplatin) formed, which correspondingly indicated the better efficacy of DD-NP (Figure 5E,F). Thereafter, the mechanism of DD-NP on in vivo PDLC model was evaluated. Severe absence of nuclei and largest necrosis area was observed in the whole area of tumor section for H&E staining after DD-NP treatment. TUNEL staining results also illustrated that combination of cisplatin and DMC in DD-NP exhibited a remarkable synergy effect on inducing apoptosis of tumor cells. Moreover, after treatment with DD-NP, tumors showed an increase in expression of P-Akt and  $\gamma$ H2AX in immunohistochemical assay, indicating the enhanced genomic DNA damage in vivo (Figure 5G). Finally, the systemic toxicity of DD-NP and SD-NP as well as small molecules was studied. H&E assay of different normal organs (Figure S28, Supporting Information) indicated that obvious

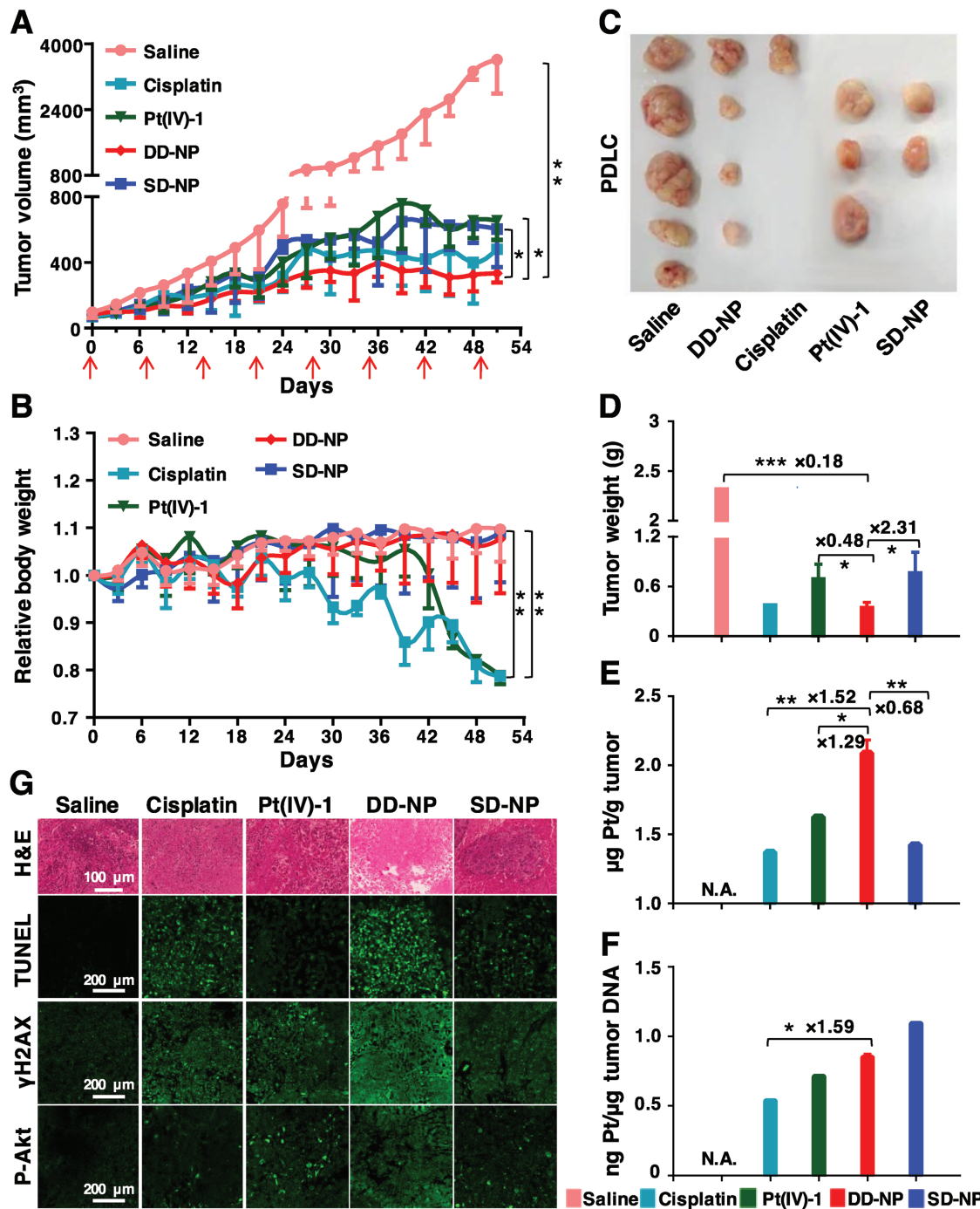


**Figure 5.** In vivo antitumor efficacy, toxicity, and action mechanism of DD-NP on BALB/c mice bearing PDLC model. The mice were administered intravenously with saline, cisplatin ( $2 \text{ mg Pt kg}^{-1}$ ), Pt(IV)-1 ( $2 \text{ mg Pt kg}^{-1}$ ), DD-NP ( $2 \text{ mg Pt kg}^{-1}$ ) and SD-NP ( $2 \text{ mg Pt kg}^{-1}$ ) on days 0, 7, 14, 21 and doubled dosages on days 28, 35, 42. A) Tumor growth curve and B) body weight change of mice during the test. C) Photo and D) tumor weight of PDX tumors isolated from mice on day 51. E) Accumulation of platinum and F) DNA-Pt adducts in tumors on day 51. Data represent mean  $\pm$  SD ( $n = 5$ ). N.A. means not available. G) H&E, TUNEL, and immunohistochemical analysis of tumor sections isolated from mice on day 51. For TUNEL and immunohistochemical assay, broken DNA strands, P-Akt, and  $\gamma$ H2AX were stained by FITC (green).

spotty necrosis, abundant inflammatory cell infiltration, and edema with thickening of the glomerular basement membrane were observed in liver for cisplatin and Pt(IV)-1 treated groups. However, DD-NP and SD-NP displayed no noticeable signals of liver and kidney damage (Figure S29, Supporting Information).

All the above results indicated that DD-NP could reduce the toxicity caused by both cisplatin and DMC.

In conclusion, to overcome the bottleneck to the clinical translation of nanomedicine, we here demonstrated a dual sensitive dual drug backbone-shattering polymeric theranostic

nanomedicine system (DD-NP). Dual synergistic drugs (Pt and DMC) combined at a precise ratio (1:2), could be triggered release from DD-NP in a chain-shattering manner under intracellular reduction/acidic microenvironment for optimal anticancer efficacy. Notably, we showed the first time of using DD-NP to eradicate the tumor burden on a high-fidelity PDLC model. Moreover, DD-NP can be applied as contrast agent to directly track the drug itself and NP via Pt DMCT and ICP-MS both in vitro and in vivo due to the exceptional high content of heavy metal Pt in polymer backbone. Our results provided the first example of personalized nanomedicine tackling the major challenges together including precise composition, direct fate monitoring of drug, drug evaluation and screening on reliable cancer models, validating the possible use of DD-NP in clinic.

## Supporting Information

Supporting Information is available from the Wiley Online Library or from the author.

## Acknowledgements

Y.C. and H.X. contributed equally to this work. The authors greatly acknowledge the financial support from National Natural Science Foundation of China (Grant Nos. 51403198, 51773198, 51673188, and 51573069), and Jilin Provincial Science and Technology Department (Grant Nos. 20150520019JH and 20170101091JC). The authors would also like to thank Prof. Yaorong Zheng at Kent University (USA) and Prof. Fuyi Wang at Institute of Chemistry, Chinese Academy of Sciences for discussion and proofreading. The animal studies were approved by the local institution review board and performed according to the Guidelines of the Committee on Animal Use and Care of Chinese Academy of Sciences.

## Conflict of Interest

The authors declare no conflict of interest.

## Keywords

computer tomography, drug delivery, nanomedicine, shattering polymers

Received: October 26, 2017

Revised: November 28, 2017

Published online: January 19, 2018

- [1] a) S. Wilhelm, A. J. Tavares, Q. Dai, S. Ohta, J. Audet, H. F. Dvorak, W. C. W. Chan, *Nat. Rev. Mater.* **2016**, *1*, 16014; b) Y. Min, J. M. Caster, M. J. Eblan, A. Z. Wang, *Chem. Rev.* **2015**, *115*, 11147; c) J. Shi, P. W. Kantoff, R. Wooster, O. C. Farokhzad, *Nat. Rev. Mater.* **2017**, *17*, 20.
- [2] a) Y. Lu, A. A. Aimetti, R. Langer, Z. Gu, *Nat. Rev. Mater.* **2016**, *2*, 16075; b) Q. Hu, W. Sun, C. Wang, Z. Gu, *Adv. Drug Delivery Rev.* **2016**, *98*, 19.
- [3] a) R. G. Tuguntaev, S. Chen, A. S. Eltahan, A. Mozhi, S. Jin, J. Zhang, C. Li, P. C. Wang, X. J. Liang, *ACS Appl. Mater. Interfaces* **2017**, *9*,

16900; b) Q. Cheng, L. Du, L. Meng, S. Han, T. Wei, X. Wang, Y. Wu, X. Song, J. Zhou, S. Zheng, Y. Huang, X. J. Liang, H. Cao, A. Dong, Z. Liang, *ACS Appl. Mater. Interfaces* **2016**, *8*, 4347; c) Q. Cheng, H. Shi, H. Huang, Z. Cao, J. Wang, Y. Liu, *Chem. Commun.* **2015**, *51*, 17536.

- [4] a) H. J. Li, J. Z. Du, J. Liu, X. J. Du, S. Shen, Y. H. Zhu, X. Wang, X. Ye, S. Nie, J. Wang, *ACS Nano* **2016**, *10*, 6753; b) W. Sun, S. Li, B. Haupler, J. Liu, S. Jin, W. Steffen, U. S. Schubert, H. J. Butt, X. J. Liang, S. Wu, *Adv. Mater.* **2017**, *29*, 1603702; c) H. J. Li, J. Z. Du, X. J. Du, C. F. Xu, C. Y. Sun, H. X. Wang, Z. T. Cao, X. Z. Yang, Y. H. Zhu, S. Nie, J. Wang, *Proc. Natl. Acad. Sci. USA* **2016**, *113*, 4164; d) M. Wang, S. Sun, C. I. Neufeld, B. Perez-Ramirez, Q. Xu, *Angew. Chem., Int. Ed.* **2014**, *53*, 13444; e) D. Zhou, J. Guo, G. B. Kim, J. Li, X. Chen, J. Yang, Y. Huang, *Adv. Healthcare Mater.* **2016**, *5*, 2493; f) J. Yang, W. Liu, M. Sui, J. Tang, Y. Shen, *Biomaterials* **2011**, *32*, 9136.
- [5] a) Y. Min, J. Li, F. Liu, E. K. L. Yeow, B. Xing, *Angew. Chem., Int. Ed.* **2014**, *53*, 1012; b) P. Ma, H. Xiao, C. Yu, J. Liu, Z. Cheng, H. Song, X. Zhang, C. Li, J. Wang, Z. Gu, J. Lin, *Nano Lett.* **2017**, *17*, 928; c) S. Han, A. Samanta, X. Xie, L. Huang, J. Peng, S. J. Park, D. B. L. Teh, Y. Choi, Y. T. Chang, A. H. Ali, Y. Yang, B. Xing, X. Liu, *Adv. Mater.* **2017**, *29*, 1700244; d) G. Song, L. Cheng, Y. Chao, K. Yang, Z. Liu, *Adv. Mater.* **2017**, *29*, 1700996; e) Q. Wu, Q. Cheng, S. Yuan, J. Qian, K. Zhong, Y. Qian, Y. Liu, *Chem. Sci.* **2015**, *6*, 6607; f) Y. Zhao, J. Peng, J. Li, L. Huang, J. Yang, K. Huang, H. Li, N. Jiang, S. Zheng, X. Zhang, Y. Niu, G. Han, *Nano Lett.* **2017**, *17*, 4096.
- [6] J. J. Tentler, A. C. Tan, C. D. Weekes, A. Jimeno, S. Leong, T. M. Pitts, J. J. Arcaroli, W. A. Messersmith, S. G. Eckhardt, *Nat. Rev. Clin. Oncol.* **2012**, *9*, 338.
- [7] a) C. Sawyers, *Nature* **2004**, *432*, 294; b) J. A. Baron, *Nat. Rev. Cancer* **2012**, *12*, 368.
- [8] a) S. Aparicio, M. Hidalgo, A. L. Kung, *Nat. Rev. Cancer* **2015**, *15*, 311; b) T. Inoue, N. Terada, T. Kobayashi, O. Ogawa, *Nat. Rev. Urol.* **2017**, *14*, 267.
- [9] a) S. Y. Choi, D. Lin, P. W. Gout, C. C. Collins, Y. Xu, Y. Wang, *Adv. Drug Delivery Rev.* **2014**, *79–80*, 222; b) H. Ledford, *Nature* **2016**, *530*, 391; c) J. Ni, S. H. Ramkissoon, S. Xie, S. Goel, D. G. Stover, H. Guo, V. Luu, E. Marco, L. A. Ramkissoon, Y. J. Kang, M. Hayashi, Q. D. Nguyen, A. H. Ligon, R. Du, E. B. Claus, B. M. Alexander, G. C. Yuan, Z. C. Wang, J. D. Iglehart, I. E. Krop, T. M. Roberts, E. P. Winer, N. U. Lin, K. L. Ligon, J. J. Zhao, *Nat. Med.* **2016**, *22*, 723.
- [10] a) J. A. Kemp, M. S. Shim, C. Y. Heo, Y. J. Kwon, *Adv. Drug Delivery Rev.* **2016**, *98*, 3; b) B. Jang, H. Kwon, P. Katila, S. J. Lee, H. Lee, *Adv. Drug Delivery Rev.* **2016**, *98*, 113; c) X. Wei, Y. Wang, X. Xiong, X. Guo, L. Zhang, X. Zhang, S. Zhou, *Adv. Funct. Mater.* **2016**, *26*, 8266.
- [11] a) Q. Chen, C. Liang, X. Sun, J. Chen, Z. Yang, H. Zhao, L. Feng, Z. Liu, *Proc. Natl. Acad. Sci. USA* **2017**, *114*, 5343; b) H. Gong, Y. Chao, J. Xiang, X. Han, G. Song, L. Feng, J. Liu, G. Yang, Q. Chen, Z. Liu, *Nano Lett.* **2016**, *16*, 2512; c) W. Zheng, Q. Luo, Y. Lin, Y. Zhao, X. Wang, Z. Du, X. Hao, Y. Yu, S. Lu, L. Ji, X. Li, L. Yang, F. Wang, *Chem. Commun.* **2013**, *49*, 10224; d) H. Huang, H. Shi, J. Liu, Y. Min, Y. Wang, A. Z. Wang, J. Wang, Y. Liu, *Chem. Commun.* **2016**, *53*, 212.
- [12] T. C. Johnstone, K. Suntharalingam, S. J. Lippard, *Chem. Rev.* **2016**, *116*, 3436.
- [13] J. Lu, J. S. Kovach, F. Johnson, J. Chiang, R. Hodes, R. Lonser, Z. Zhuang, *Proc. Natl. Acad. Sci. USA* **2009**, *106*, 11697.
- [14] D. Zhou, H. Xiao, F. Meng, X. Li, Y. Li, X. Jing, Y. Huang, *Adv. Healthcare Mater.* **2013**, *2*, 822.
- [15] C. Y. Sun, S. Shen, C. F. Xu, H. J. Li, Y. Liu, Z. T. Cao, X. Z. Yang, J. X. Xia, J. Wang, *J. Am. Chem. Soc.* **2015**, *137*, 15217.
- [16] a) H. Xiong, D. Zhou, X. Zheng, Y. Qi, Y. Wang, X. Jing, Y. Huang, *Chem. Commun.* **2017**, *53*, 3422; b) J. Chen, J. Ding, Y. Wang, J. Cheng, S. Ji, X. Zhuang, X. Chen, *Adv. Mater.* **2017**, *29*, 1701170.

- [17] a) J. M. Houthuijzen, L. G. Daenen, J. M. Roodhart, I. Oosterom, M. T. van Jaarsveld, K. M. Govaert, M. E. Smith, S. J. Sadatmand, H. Rosing, F. Kruse, B. J. Helms, N. van Rooijen, J. H. Beijnen, B. Haribabu, C. H. van de Lest, E. E. Voest, *Nat. Commun.* **2014**, *5*, 5275; b) Z. Z. Yu, W. Pan, N. Li, B. Tang, *Chem. Sci.* **2016**, *7*, 4237.
- [18] Z. Zhang, S. Liu, Y. Qi, D. Zhou, Z. Xie, X. Jing, X. Chen, Y. Huang, *J. Controlled Release* **2016**, *235*, 125.
- [19] a) X. Han, J. Sun, Y. Wang, Z. He, *Med. Res. Rev.* **2015**, *35*, 1268; b) M. D. Hall, T. W. Hambley, *Coord. Chem. Rev.* **2002**, *232*, 47.
- [20] S. Dhar, N. Kolishetti, S. J. Lippard, O. C. Farokhzad, *Proc. Natl. Acad. Sci. USA* **2011**, *108*, 1850.
- [21] Y. Liu, K. Ai, J. Liu, Q. Yuan, Y. He, L. Lu, *Angew. Chem., Int. Ed.* **2012**, *51*, 1437.